

A Novel Continuum-Style Robot with Multilayer Compliant Modules

Peng Qi, Chen Qiu, Hongbin Liu, Jian S. Dai, Lakmal Seneviratne, Kaspar Althoefer

Abstract— This paper introduces a novel continuum-style robot that integrates multiple layers of compliant modules. Its essential features lie in that its bending is not based on natural compliance of a continuous backbone element or soft skeletal elements but instead is based on the compliance of each structured planar module. This structure provides several important advantages. First, it demonstrates a large linear bending motion, whilst avoiding joint friction. Second, its contraction and bending motion are decoupled. Third, it possesses ideal back-drivability and a low hysteresis. We further provide an analytical method to study the compliance characteristics of the planar module and derive the statics and kinematics of the robot. The paper provides an overview of experiments validating the design and analysis.

I. INTRODUCTION AND BACKGROUND

Continuum-style robots, including those inspired by biology, increasingly arouse the attention of researchers due to the compliance capability and the wide range of motion. In the last two decades, there have been remarkable developments: many new designs appeared and various applications in both medical and industrial fields were demonstrated [1]. The related scientific problems range from designing and modeling to low-level control and high-level task execution. Compared to modular rigid-link robots, continuum-style robots are more diverse, often resembling animals or animal appendages, such as snakes, elephant trunks and octopus tentacles [2].

Historically, the first continuum-style robot is generally accepted to be Anderson and Horn's tensor arm manipulator invented in the late 1960s [3] – a tendon-driven spine-like flexible arm. Subsequently in 1971, Hirose started to propose creative designs of snake-like robots and appropriate control systems based on the biomechanical study of snakes [2]. Early works also include Chirikjian's pilot research in the 1990s on establishing the fundamental modeling technique to formulate the dynamics of hyper-redundant manipulators [4]. The late 1990s and the 2000s saw an increasing trend of miniature continuum-style robots being moved into robotic surgery with a view to finding solutions for robot-assisted minimally invasive surgery with its inherent access problems through small incisions [5]. Meanwhile, soft robotics as a subset of continuum-style robotics emerged with the development of novel soft actuators and sensors [6]. Most recently, Walker [1] reviewed the state of art of continuous backbone robot manipulators and analyzed the hardware design principles that inspired our work.

A continuum robot can be identified with a continuous backbone structure. However, a hyper-redundant robot [4]

sometimes also has an external continuous appearance which is comprised of a segmented backbone with many short rigid links; hence, the latter types of robots, strictly speaking, do not represent truly continuum robots but will be termed "continuum-style robots" here. Herein, we summarize the frequently applied continuum-style robot constructions to date according to the distinctive backbone architecture, but excluding the subset of "invertebrate" soft robots. Of these, the early robot construction is composed of serially connected independent joints, which pertains to the aforementioned hyper-redundant manipulator. The designs share the advantages of having a large number of degrees of freedom (DOFs) and accurate control, however they suffer from the problems of lighter payload, joint friction and incompressibility/inextensibility.

Perhaps the most common form of truly continuum robots is to use a spring backbone [3]. Due to the flexibility of the spring structure, the shape of a robot can be actuated in a tendon-driven manner and allows an ideal back-drivability and a relatively low hysteresis. However, its compression and the bending deflection are mechanically coupled, leading to a bending actuation that is partially lost in compression [1]. Another popular design of continuum robots utilizes a laterally super-elastic, but longitudinally incompressible rod/tube as the backbone element [7]. A distinctive feature of using an elastic central backbone is design simplicity. On top of this, both control and modeling will be straightforward. They consistently can be formulated by beam-mechanics-based models. It is in this regard that active cannulas [8] also falls into this category. Despite our classification illustrating the diversity of designs, there do not exist strict boundaries among various kinds of continuum-style robots. For example, a spring-based continuum robot sometimes is integrated with an elastic rod as the incompressible central backbone to diminish the natural compliance.

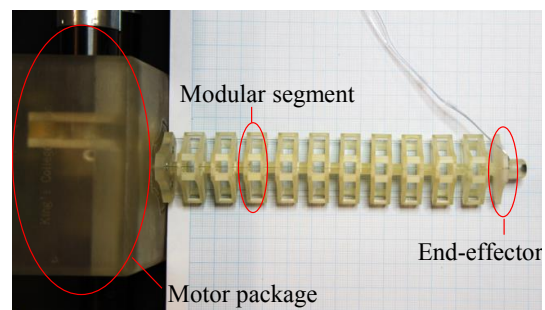


Figure 1. A multi-layer structured continuum-style robot.

In this paper, we propose a design of continuum-style robot that has multiple layers of compliant planar modules linked in series (see Fig. 1). Its essential features lie in that the bending of this continuum-style robot is not based on natural compliance of a continuous backbone element or soft skeletal elements but utilizes the compliance of each structured planar module. The main advantages of using compliant planar

P. Qi, C. Qiu, H. Liu, J. S. Dai, and K. Althoefer are with the Centre for Robotics Research, Department of Informatics, King's College London, WC2R 2LS, UK. (e-mail: peng.qi@kcl.ac.uk)

L. Seneviratne is with Khalifa University, Abu Dhabi, UAE and Emeritus Professor of Mechatronics, King's College London, UK.

modules are due to their linear output motion and avoiding friction between joints. We present an analytical method to study the compliance characteristics of the planar module and derive the compliance matrix to represent the force-deflection relationships, thus making the linear motion accurately predictable. Another advantage of the continuum-style robot (Fig. 1) is owing to the serial connection of the conjoined layers, thus demonstrating a large linear bending motion, although the linear-motion approximation of one layer only holds under the condition of small deflections. Additionally, the structure is back-drivable – a desirable feature in robotics and improving safety when operating in close vicinity of humans. This structure behaves like a helical spring, but its contraction and bending motion are decoupled, thus reducing the uncontrolled compression when generating normal deflections. This feature renders the bending of the robot more controllable. Besides, it has the capability of maintaining better structural rigidity of the whole continuum body when compared to a spring-backbone-based design, and thus convinces with comparatively low hysteresis.

II. CONCEPTUAL DESIGN OF THE ROBOT

A. Segment Design

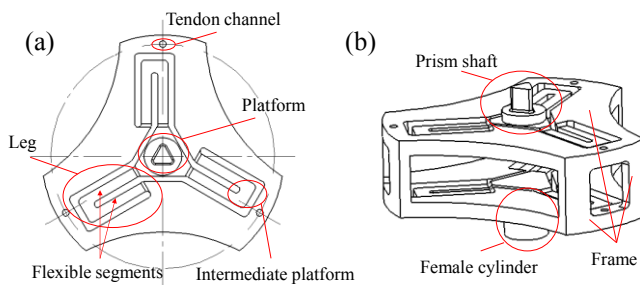


Figure 2. Design of double-layer modular segment. (a) Top view; (b) Side view.

Fig. 2(a) depicts a top view of the compliant planar module. Howell et al. first constructed similar types of designs and identified different configurations [9]. Due to its out-of-plane motion along an axis orthogonal to the parent plane, these devices are also called “ortho-planar springs” [9]. In Fig. 2(a), the design is presented in detail: three legs (120° apart) radially extend away from the central platform and are anchored to the outer base; each leg has two flexible segments shaped like a “U” (U-shape design); the intermediate platform is considered infinitely stiff. In the current design the circular outer contour has a 29mm diameter and the length of each leg is 8mm. The thickness of the flexible beam elements is 1mm; the width 1.2mm and both can be varied to change the beam compliance. Part of the base is cut in order to reduce the mass. Three tendon channels with a 0.8mm diameter are reserved for guiding tendons through each layer of modules. They are positioned on the far edge of the base and along the extension line of the leg. This compliant layer possesses one DOF to raise and lower the platform relative to the fixed base and 2 DOFs to allow the platform to freely perform titling motions around the center, thus 3 DOFs in total. A three-legged design is chosen for the reason that it is the minimum odd number leg count, which allows reducing the rotational tendencies of each leg and increasing the stability of the platform [9]. The radial

structure causes the central platform to undergo large deflections when a given moment is applied to the center.

Fig. 2(b) depicts the modular segment design for our continuum-style robot. It integrates two layers of compliant planar modules facing opposite directions; a prism-like shaft and a mating female cylinder are respectively fixed on each platform of the top and the bottom. The polygonal cross-section design of the axial coupling resists relative rotation between the two segments and while enabling torque transmission. They are fitted precisely to connect from segment to segment. Except for the flexible segments and the two platforms with their “vertebrae”, any other part of the segment is a part of the frame extending from the base to the tip of the manipulator; this frame is idealized to be a rigid body. When fixing the bottom cylinder, if a load is applied to the prism shaft, the relative displacement or rotation of two platforms would be double compared to that of one layer for the same load. The gap between the two layers currently is 5mm, providing enough space to keep the outer edges of two legs or two platforms of the top and bottom layers from colliding. The segmented modular design allows the length of the continuum-style robot to cope with various intended, bending scenarios.

B. Continuum-Style Robot Assembly

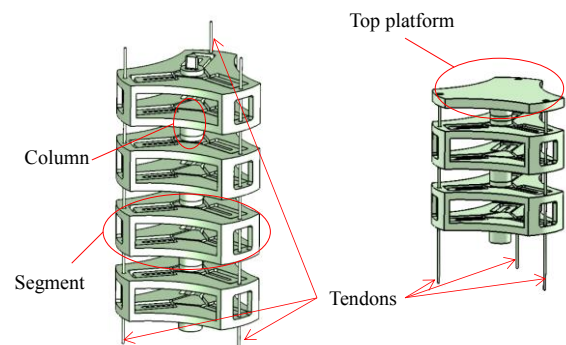


Figure 3. Partial views of continuum-style robot assembly.

The current continuum-style robot prototype consists of 10 modular segments. Fig. 3 shows partial views of the assembly. Including a distal plate and a bottom support, the total length is 143mm. The distance between the lower face of one segment and the upper face of the subsequent segment is 5mm, the same as the gap between the two layers of one segment. Three tendons are routed along the aligned segments through the tendon channels and secured to the distal plate, which leads to a tendon-driven under-actuated design. The rigid distal plate can be regarded as an extension of the last platform. By pulling the tendons, the load will be transmitted from the distal platform to the proximal bottom support, thus generating compression and steering motions. Moreover, depending on the intended operations, additional groups of tendons can be used to increase the mobility and functionality. They are secured to some selected point of column and produce torques to the lower part.

III. COMPLIANCE OF PLANAR MODULE

From the perspective of mechanical design, the planar module is a type of hybrid flexure mechanisms [9]. Each flexible segment in each leg can be treated as a beam flexure. Each leg is a folded serial chain of two fixed-guided beam

flexures. The planar module is formed by connecting the central platform to the outer base through three legs in parallel. Thus, we can stepwise derive the compliance matrix for the entire module with a bottom-up approach.

A. Compliance Matrix Derivation

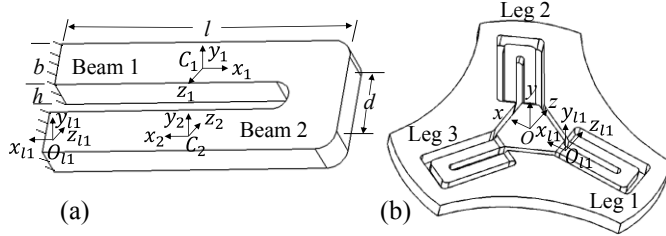


Figure 4. Coordinate frame transformation. (a) One leg of the design; (b) A compliant layer.

Fig. 4(a) depicts one leg of the design. The small deformation of each beam is defined as a twist deflection, which in ray coordinates can be denoted by

$$\mathbf{S} = [\theta_x \ \theta_y \ \theta_z \ \delta_x \ \delta_y \ \delta_z]^T \quad (1)$$

where the first group of three elements represents the three rotational deflections about their corresponding axes, whilst the last three elements reveal the corresponding translational deflections. A twist deflection \mathbf{S} is an element of the Lie algebra $se(3)$ of Lie group $SE(3)$.

And in harmony with this, the loading force is considered as a general wrench in axis coordinates

$$\mathbf{W} = [m_x \ m_y \ m_z \ f_x \ f_y \ f_z]^T \quad (2)$$

in which the primary part $\mathbf{m} = [m_x \ m_y \ m_z]^T$ is the vector attached with the force amplitude, representing the direction of the axis of the wrench, whilst the location of the axis of the wrench is given by the secondary part $\mathbf{f} = [f_x \ f_y \ f_z]^T$. A wrench is an element of the dual Lie algebra $se^*(3)$.

Consider beam 1 of the leg in Fig. 4(a), a local coordinate frame $\{x_1 y_1 z_1\}$ generally can be established at the centroid of the beam. With the coordinates of both the twist deflection and the wrench written in the same frame $\{x_1 y_1 z_1\}$, then the compliance matrix of beam 1 can be derived [10] and expressed as

$$\mathbf{C}_1 = \text{diag} \left[\frac{l}{GJ} \quad \frac{l}{EI_y} \quad \frac{l}{EI_z} \quad \frac{l}{EA} \quad \frac{l^3}{12EI_z} \quad \frac{l^3}{12EI_y} \right] \quad (3)$$

where the primary part represents torsional compliance and the secondary part the linear compliance. As shown in Fig. 4, beam 1 has a rectangular cross-section with the width b and the thickness h ($b > h$), as well as a length l , and the area of the cross-section A is equal to bh . E denotes the elastic module of the material, and G denotes the shear module of the material with $G = E/(2(1+\nu))$ and ν Poisson's ratio. $I_y = b^3 h/12$ and $I_z = b h^3/12$ are the moments of inertia of the beam at the cross-section with respect to axis y and axis z , and J is the torsional moment of inertia.

Equivalent results are also produced in references [10], [11], [12] and there exists remarkable similarity, however, due to coordinate frame choices, they are diverse in form.

The compliance characteristics of an individual link or a whole mechanism system are their intrinsic properties, but notice that the expression of the compliance matrix may vary and it depends on the coordinate choice. Once the coordinate system is defined, it also applies for the references when analyzing the twist deflection of a finite segment.

For (1), (2) and (3), we have the relations between a twist deflection and a loading wrench summarized below

$$\mathbf{S} = \mathbf{C}_1 \mathbf{W} ; \mathbf{W} = \mathbf{K}_1 \mathbf{S} ; \mathbf{C}_1 = \mathbf{K}_1^{-1} \quad (4)$$

where \mathbf{K}_1 is the stiffness matrix.

Beam 2 is an identical flexible segment to beam 1, thus the compliance matrix is the same but written in its own local coordinate frame $\{x_2 y_2 z_2\}$. Two beams in the leg are connected by an intermediate platform, but it is modeled as a fixed pin joint with its compliance ignored when we consider the force-deflection relationship of the leg [9]. At the connecting edge between the leg and the platform, we established the global coordinate frame $\{x_{11} y_{11} z_{11}\}$. To shift the local coordinate frame of each beam into the global coordinate frame $\{x_{11} y_{11} z_{11}\}$, an adjoint action of Lie group $SE(3)$ on its Lie algebra is introduced through a 6×6 matrix representation [13]

$$\mathbf{Ad}_g = \begin{bmatrix} \mathbf{R} & \mathbf{0} \\ \mathbf{A}\mathbf{R} & \mathbf{R} \end{bmatrix} \quad (5)$$

where \mathbf{R} is a 3×3 rotation matrix of the coordinate transformation, and \mathbf{A} is a skew-symmetric matrix spanned by translation vector \mathbf{d} .

Then, the coordinates of a twist deflection and a wrench in the coordinate frame $\{x_{11} y_{11} z_{11}\}$ are calculated as [10], [12]

$$\mathbf{S}' = \mathbf{Ad}_g \mathbf{S} ; \mathbf{W}' = \mathbf{Ad}_g^{-T} \mathbf{W} \quad (6)$$

To obtain the compliance matrix \mathbf{C}' in the new coordinate frame, we deduct it as follows based on (4):

$$\mathbf{S}' = \mathbf{Ad}_g \mathbf{S} = \mathbf{Ad}_g (\mathbf{C}\mathbf{W}) = \mathbf{Ad}_g \mathbf{C} \mathbf{Ad}_g^T \mathbf{W}' \quad (7)$$

Thus, we derive that the compliance matrix will be transformed to the new coordinate frame according to the relation

$$\mathbf{C}' = \mathbf{Ad}_g \mathbf{C} \mathbf{Ad}_g^T \quad (8)$$

Similarly, we can derive the stiffness matrix in the new coordinate frame $\{x_{11} y_{11} z_{11}\}$ as

$$\mathbf{K}' = \mathbf{Ad}_g^{-T} \mathbf{K} \mathbf{Ad}_g^{-1} \quad (9)$$

Here, the inverse and the inverse transpose of such adjoint transformation matrix are given respectively by

$$\mathbf{Ad}_g^{-1} = \begin{bmatrix} \mathbf{R}^T & \mathbf{0} \\ -\mathbf{R}^T \mathbf{A} & \mathbf{R}^T \end{bmatrix} ; \mathbf{Ad}_g^{-T} = \begin{bmatrix} \mathbf{R} & \mathbf{A}\mathbf{R} \\ \mathbf{0} & \mathbf{R} \end{bmatrix} \quad (10)$$

All deformations are written in the same coordinate frame $\{x_{11} y_{11} z_{11}\}$, then the overall compliance matrix of the leg as a serial flexure chain is obtained [12] by

$$\mathbf{C}_{l1} = \sum_{i=1}^2 (\mathbf{Ad}_g)_i \mathbf{C}_i (\mathbf{Ad}_g)_i^T, \quad (i=1, 2). \quad (11)$$

Given a compliance matrix of one leg, its corresponding stiffness matrix $\mathbf{K} = \mathbf{C}^{-1}$ is first calculated. It is noted that all

twist deflections and wrenches here must be transformed into the same coordinate frame, and correspondingly, the stiffness matrix of each leg will be expressed in such a global coordinate frame. We establish the global coordinate frame $\{xyz\}$ in the center of the triangular platform, see Fig. 4(b). The radius of the plate is labeled by parameter r . The coordinate transformation operation from the connecting edge between the leg and the platform, i.e. the edge of the disc to the center of disc follows the aforementioned relation in (9). Further considering that the overall layer's stiffness is isotropic [14], it gives the unified form as

$$\mathbf{K}_0 = \mathbf{K}'_1 + \mathbf{N}\mathbf{K}'_1\mathbf{N}^T + \mathbf{N}^2\mathbf{K}'_1\mathbf{N}^{2T} \quad (12)$$

where \mathbf{K}'_1 is the stiffness matrix of leg 1 in the global coordinate frame $\{xyz\}$; it is derived by the relation $\mathbf{K}'_1 = \mathbf{T}^T\mathbf{K}_1\mathbf{T}$ based on (9), which indicates a coordinate transformation from the local coordinate frame at the connecting edge to the global coordinate frame of the platform center. In the case, \mathbf{T} only possesses the translation action along the x axis. \mathbf{N} describes the rotation action based on the fact that three legs are symmetrically connected to the platform with an angle 120° .

Finally, the compliance matrix of the overall planar module layer as a type of hybrid flexure mechanisms is computed by inverting the stiffness matrix \mathbf{K}_0 ,

$$\mathbf{C}_0 = \mathbf{K}_0^{-1} = \begin{bmatrix} c_{11} & 0 & 0 & 0 & 0 & 0 \\ 0 & c_{22} & 0 & 0 & 0 & 0 \\ 0 & 0 & c_{33} & 0 & 0 & 0 \\ 0 & 0 & 0 & c_{44} & 0 & 0 \\ 0 & 0 & 0 & 0 & c_{55} & 0 \\ 0 & 0 & 0 & 0 & 0 & c_{66} \end{bmatrix} \quad (13)$$

Here, the nonzero compliance elements are denoted by the variables with two subscripts. They are all determined by both material parameters and geometric parameters of the mechanical design of the compliant layer structure.

B. Compliance Analysis and Numerical Example

The compliance matrix in (13) is symmetric positive definite (SPD), and the diagonal entries represent the translational and rotational compliance in/about all directions, respectively. Besides, all diagonal compliance elements of \mathbf{C}_0 can factor out a factor that coincides with the corresponding elements of beam's compliance matrix in (3). By observing compliance elements of \mathbf{C}_0 , we notice that the x - z planar motion (x, z, θ_y) is decoupled from out-of-plane forcing and vice-versa. On the other hand, the entries outside the main diagonal are all zero, revealing that the out-of-plane rotation and translational motion of the platform are decoupled. This further verifies that the contraction effort and bending motion of the multi-layer structured continuum-style robot will be theoretically independent to each other.

In the following, we use two numerical examples to further reveal the information embodied in the compliance matrix. The dimensions of the planar module are $l=8\text{mm}$, $b=1.2\text{mm}$, $h=1\text{mm}$, $d=2\text{mm}$, $r=3.5\text{mm}$. Aluminum alloy (Young's module $E=71\text{GPa}$ and Poisson's ratio $\nu=0.33$) and polyethylene ($E=1.1\text{GPa}$ and $\nu=0.42$) are selected as fabrication material for use in the two examples, respectively, thus deriving each

element of the corresponding numerical compliance matrix as tabulated in Table 1.

Table 1. Numerical examples of compliance elements.

Compliance element	Aluminum alloy	Polyethylene
c_{11}	1.39×10^{-1}	9.54
c_{22}	4.19×10^{-2}	2.71
c_{33}	1.39×10^{-1}	9.54
c_{44}	9.66×10^{-7}	6.23×10^{-5}
c_{55}	4.82×10^{-6}	3.28×10^{-4}
c_{66}	9.66×10^{-7}	6.23×10^{-5}

By analyzing the numerical results, we can draw the following conclusions.

1. In the group of rotational compliance elements (c_{11} , c_{22} and c_{33}), the rotational compliance elements both c_{11} and c_{33} about the horizontal x and z axis are more than 3 times larger than the rotational compliance element c_{22} about the vertical axis y , indicating its potential to be used for bending motions in continuum-style robot, while resisting in-plane rotations.

2. In the group of translational compliance elements (c_{44} , c_{55} and c_{66}), the vertical compliance element c_{55} is about 5 times larger than both the horizontal compliance element c_{66} along z axis and the horizontal compliance element c_{44} along x axis. This result agrees with our intuition and the qualitative study by Howell et al. [9]. Such translational motion along the vertical axis of the planar module has been investigated for use in many applications, such as a pneumatic valve controller for Flowserve [9] and a force sensor [15].

Overall, c_{11} , c_{33} and c_{55} are the major compliance elements. Thus, reasonably, further analysis can focus on the major displacements θ_x , θ_z and δ_y that are produced by the loads m_x , m_z and f_y , respectively.

IV. STATICS ANALYSIS AND KINEMATIC MODELING

First of all, there arise three assumptions. One is that only flexible beams provide elasticity while all the rest of parts are considered to be rigid body. Another is that the effect of gravity is neglected. The third one is that the loads exerted on the top plane are uniformly distributed to each segment of the robot.

As pointed out earlier, only the two rotational deflections θ_x , θ_z and the longitudinal displacement δ_y are the main deformation corresponding to the three major compliance elements c_{11} , c_{33} and c_{55} . Thus, simplifying:

$$\begin{bmatrix} n \cdot \theta_x \\ n \cdot \theta_z \\ n \cdot \delta_y \end{bmatrix} = \begin{bmatrix} c_{11} & 0 & 0 \\ 0 & c_{33} & 0 \\ 0 & 0 & c_{55} \end{bmatrix} \begin{bmatrix} M_x \\ M_z \\ F_y \end{bmatrix} \quad (14)$$

where M_x , M_z and F_y denote the loads on the system as a whole; n is the number of compliant layers.

In this tendon-driven design, the loads are applied to the top plane via three non-stretchable tendons. Pre-tightening force will be applied, thus, activating one or two tendons, can result in rotational deflection and equally activating three tendons together leads to longitudinal compression.

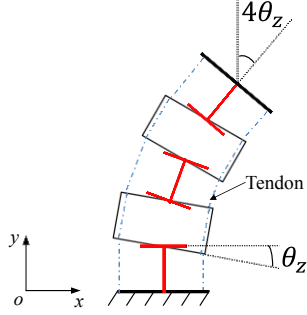


Figure 5. Configuration of two segments assembly 2D bending.

Fig. 5 shows a bending configuration of the planar model in the xy -plane, where the base of the robot is centered about the origin and the coordinate system orientation parallel to the global coordinate frame of the proximal layer. For simplicity, we only assembled two planar modules, Fig. 5. The bending of this continuum-style robot is utilizing the local beam deflection of each compliant planar module, thus we do the calculations based on the rotational deflection angle to derive the length changes of the three tendons. Firstly, we calculate the length of inner and outer boundaries of the planar model.

$$L_s = L - 2N \cdot \Delta \quad ; \quad L_l = L + 2N \cdot \Delta \quad (15)$$

where L_s and L_l denote the length of inner and outer boundaries of the planar model, respectively; L is constant, representing the initial length of this continuum-style robot; N is the number of the double layered modular segment, Fig. 2(b); Δ denotes the spacing changes of segments and $\Delta = R \sin \theta$, where θ is the generalized rotational deflection angle of each compliant layer and R is the distance from the tendon channel to the center of the plane.

In the example of Fig. 5, the structure is bending about the z axis, and the inner boundary corresponds exactly to one of the tendons on the x -axis. Later, we can obtain the rest of another two tendon lengths based on spatial model with the known distances of inner and outer boundaries.

Because the gap between the two layers of a modular segment is unchanged, we can only consider the spatial configuration of the gap between the two adjacent segments connected by a column, which is shown in Fig. 6.

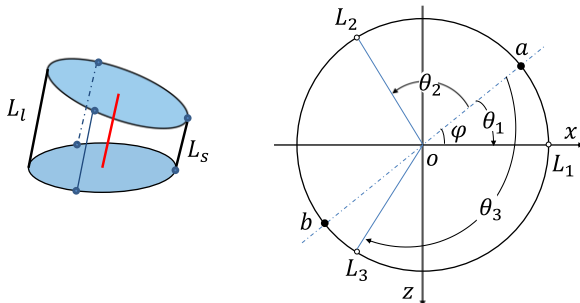


Figure 6. 3D bending geometry and cross-section area.

Besides, from the cross-sectional geometry of Fig. 6, the positional relation between the inner and outer boundaries

and the three tendons can be expressed in terms of the relative orientation φ between the two adjacent segment surfaces [16]. The orientation φ is the resultant of both θ_x and θ_z . We can calculate the lengths of three tendons based on the angular relationship, as follows:

$$L_k = L_s + \frac{\theta_k}{\pi} (L_l - L_s) - 2N \cdot \delta_y \quad , \quad (k=1,2,3) \quad (16)$$

where $2N \cdot \delta_y$ denotes the total longitudinal compression of this continuum-style robot; k identifies the tendon.

Referring back to Fig. 5, given the rotational deflection θ_z and the segment number N , the tip position of such design on the xy -plane can be calculated to be

$$\begin{bmatrix} x \\ y \\ z \end{bmatrix} = \begin{bmatrix} (g - \delta_y) \cdot (\sin \theta_z + \sin(2\theta_z) + \dots + \sin(2N\theta_z)) \\ (g - \delta_y) \cdot (1 + \cos \theta_z + \cos(2\theta_z) + \dots + \cos(2N\theta_z)) \\ 0 \end{bmatrix} \quad (17)$$

where g denotes the distance between the lower face of one segment and the upper face of the subsequent segment. Here, the equation involves the longitudinal displacement δ_y for the case of that the axial compression is generated.

After that, we rotate the planar model about the y -axis with an angle ω and obtain a spatial model. The derivation of spatial position coordinates is obtained by rotating the xy positions about the y -axis. The tip position in space is then given by multiplying the rotation matrix $R(\omega)$ and (17), yielding

$$\begin{bmatrix} x \\ y \\ z \end{bmatrix} = (g - \delta_y) \begin{bmatrix} \cos \omega \cdot (\sin \theta_z + \sin(2\theta_z) + \dots + \sin(2N\theta_z)) \\ 1 + \cos \theta_z + \cos(2\theta_z) + \dots + \cos(2N\theta_z) \\ -\sin \omega \cdot (\sin \theta_z + \sin(2\theta_z) + \dots + \sin(2N\theta_z)) \end{bmatrix} \quad (18)$$

The occurrence of the rotation is a synergistic effect of both rotational deflections $2N\theta_z$ about the z -axis and $2N\theta_x$ about the x -axis. It can be derived as

$$\omega = \arctan \frac{\theta_x}{\theta_z} \quad (19)$$

We have now found the positions of the continuum-style robot tip as functions of the three major displacements θ_x , θ_z and δ_y , thus completing the kinematics model. With the calculated tendon lengths, we have derived a model that could be used to control this continuum-style robot.

V. PROTOTYPE EXPERIMENT

A prototype of the multilayer structured continuum-style robot was tested; test procedures and results are described in this section. The double-layered segment is made of acrylonitrile butadiene styrene (ABS) plastic material and is 3D printed using a rapid prototyping machine (VisiJet[®] EX200). Besides, a mini-camera (NanEye Stereo, AWAIBA[®]) holder is designed and printed to realize a possible application of the robot as an example (here: an endoscopic camera). The length of the assembled prototype is 150mm and its diameter is 29mm. Each tendon is driven by a DC motor (Maxon Motor[®])

with a pulley; the employed 128:1 reduction gearhead allows tendon actuation with a high rotational resolution. Due to the limited compliance of the fabrication material, the prototype only serves as a preliminary setup for the investigation of the performance of hysteresis, back-drivability and bending motions.

Fig. 7 shows a comparison after and before of the longitudinal contraction, which indicates the back-drivability and to some extent ensures the safety when interacting with environments. We can also observe that the tendons' pulling force is equally distributed to each of the compliant layers and results in equal longitudinal displacements.

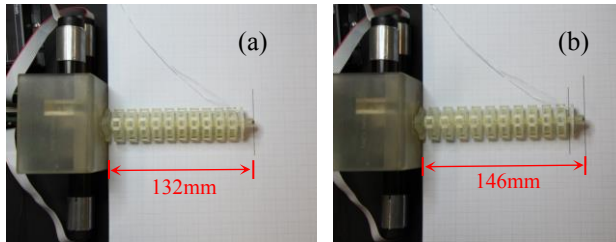


Figure 7. (a) After and (b) before longitudinal contraction.

Fig. 8(a) shows a 2D bending motion of the robot. The bending control effort does not generate compressions, which verifies that its contraction and bending motion are decoupled in the unique design. In addition, the equally distributed bending deformations are also presented here; compared with the sketch in Fig. 5, we can see that the experimental performance is virtually coinciding with the model. Fig. 8(b) shows a 3D bending motion of the robot. Some bending nonlinearity is observable, which we suspect to be because of the influence of gravity and the nonlinear stress due to non-homogenous material properties.

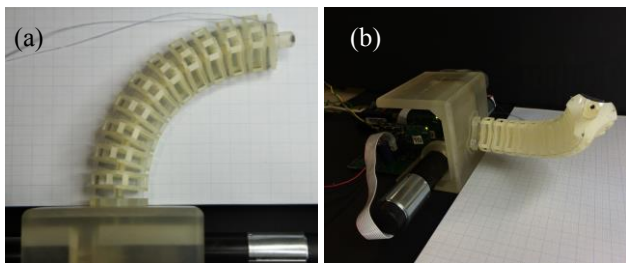


Figure 8. Bending deformation of the robot; (a) 2D bending motion; (b) 3D bending motion.

VI. CONCLUSIONS AND FUTURE WORK

This paper presents the design of a continuum-style robot with multiple layers of compliant planar modules linked in series. Firstly, we reviewed frequently applied continuum-style robot constructions to date based on the distinctive backbone architecture. Through our study, we found that our structure has advantages over other existing traditional continuum-style robot: a large linear bending motion, avoidance of joint friction, back-drivability, largely decoupled contraction and bending motions as well as low hysteresis.

We derived the compliance matrix of the planar module and provided statics and kinematics descriptions for the overall robot construction. We built and tested a prototype and observed its performance. The experimental results verified some of the characteristics of the robot, such as contraction, equally distributed longitudinal/bending displacements and decoupling.

A finite element method (FEM) analysis is being conducted to further confirm the predicted behavior of the presented continuum-style robot and subsequently a quantitative empirical validation. In the view of that the compliance characteristics of the planar module are determined by both material parameters and geometric parameters of the mechanical design, we aim to test different fabrication materials and other layer configuration, such as side-leg design and changing the number of flexible segments.

ACKNOWLEDGMENT

The work described in this paper was partially funded by European Commission's Seventh Framework Programme under grant agreement 287728 in the framework of EU project STIFF-FLOP and the China Scholarship Council.

REFERENCES

- [1] I. D. Walker, "Continuous backbone "continuum" robot manipulators," ISRN Robotics, vol. 2013, Article ID 726506, 19 pages, 2013.
- [2] S. Hirose, *Biologically Inspired Robots*, Oxford University Press, 1993.
- [3] V. C. Anderson and R. C. Horn, "Tensor arm manipulator design," *Transactions of the ASME*, vol. 67, DE-57, pp. 1-12, 1967.
- [4] G. S. Chirikjian, "Hyper-redundant manipulator dynamics: a continuum approximation," *Advanced Robotics*, 9(3), 217-243, 1994.
- [5] D. B. Camarillo, T. M. Krummel and J. K. Salisbury, "Robotic Technology in Surgery: Past, Present, and Future", *American J. of Surgery*, vol. 188, no. 4A, pp. 2-15, 2004.
- [6] D. Trivedi, C. D. Rahn, W. M. Kier, and I. D. Walker, "Soft robotics: biological inspiration, state of the art, and future research," *Applied Bionics and Biomechanics*, vol. 5, no. 3, pp. 99-117, 2008.
- [7] N. Simaan, "Snake-like units using flexible backbones and actuation redundancy for enhanced miniaturization," in *Proc. of IEEE International Conf. on Robotics and Automation*, pp. 3012-3017, 2005.
- [8] R. J. Webster, R. Joseph, N. J. Cowan, "Mechanics of precurved-tube continuum robots," *IEEE Trans. on Robotics*, 25(1), pp. 67-78, 2009.
- [9] J. J. Parise, L. L. Howell, S. P. Magleby, "Orthoplanar linear-motion springs," *Mechanism and machine theory*, 36(11), 1281-1299, 2001.
- [10] J. Selig and X. Ding, 2001, "A Screw Theory of Static Beams," in *Proceedings of the 2001 IEEE/IROS*, vol. 1, pp. 312-317, 2001.
- [11] X. Ding, J. S. Dai, "Compliance analysis of mechanisms with spatial continuous compliance in the context of screw theory and lie groups," *Journal of Mechanical Engineering Science* 224.11 (2010): 2493-2504.
- [12] H.-J. Su, H. Shi, and J. Yu, "A symbolic formulation for analytical compliance analysis and synthesis of flexure mechanisms", *J. of Mechanical Design*, 134, p. 051009, 2012.
- [13] J.S. Dai, "Finite Displacement Screw Operators with Embedded Chasles' Motion." *J. Mechanisms Robotics*, 4(4), 041002, 2012.
- [14] J. S. Dai, and X. Ding, "Compliance analysis of a three-legged rigidly-connected platform device," *Journal of Mechanical Design*, vol. 128, no. 4, pp. 755-764, 2006.
- [15] A. Ataollahi, A. Fallah, L. Seneviratne, P. Dasgupta, and K. Althoefer. "Novel Force Sensing Approach Employing Prismatic-Tip Optical Fiber Inside an Orthoplanar Spring Structure", *IEEE/ASME Transactions on Mechatronics*, vol. 19, no. 1, pp. 1-10, 2012.
- [16] D. G. Choi, B.-J. Yi, and W.-K. Kim, "Design of a Spring Backbone Micro Endoscope," in *Proc. of IEEE/RSJ International Conf. on Intelligent Robots and Systems*, pp. 1815-1821, 2007.